

Turbulence statistics of a Kelvin–Helmholtz billow event observed in the night-time boundary layer during the Cooperative Atmosphere–Surface Exchange Study field program

William Blumen^{a,*}, Robert Banta^b, Sean P. Burns^c,
David C. Fritts^d, Rob Newsom^e, Gregory S. Poulos^d, Jielun Sun^{a,c}

^a Program in Atmospheric and Oceanic Sciences (PAOS), University of Colorado, Boulder, CO 80309, USA

^b Environmental Technology Laboratory/NOAA, 325 Broadway, Boulder, CO 80305, USA

^c National Center for Atmospheric Research (NCAR), P.O. Box 3000, Boulder, CO 80307-3000, USA

^d Colorado Research Associates (CoRA)/Northwest Research Associates (NWRA),
3380 Mitchell Lane, Boulder, CO 80301, USA

^e Cooperative Institute for Research in the Atmosphere, Colorado State University, Fort Collins, CO 80523, USA

Received 21 September 2000; received in revised form 9 March 2001; accepted 14 March 2001

Abstract

An apparent shear flow instability occurred in the stably stratified night-time boundary layer on 6 October 1999 over the Cooperative Atmosphere–Surface Exchange Study (CASES-99) site in southeast Kansas. This instability promoted a train of billows which appeared to be in different stages of evolution. Data were collected by sonic anemometers and a high-frequency thermocouple array distributed on a 60 m tower at the site, and a high resolution Doppler lidar (HRDL), situated close to the tower. Data from these instruments were used to analyze the characteristics of the instability and the billow event. The instability occurred in a layer characterized by a minimum Richardson number $Ri \sim 0.13$, and where an inflection in the background wind profile was also documented. The billows, which translated over the site for approximately 30 min, were approximately $L \sim 320$ m in length and, after billow evolution they were contained in a layer depth $H \sim 30$ m. Their maximum amplitude, determined by HRDL data, occurred at a height of 56 m. Billow overturns, responsible for mixing of heat and momentum, and high-frequency intermittent turbulence produce kurtosis values above the Gaussian value of 3, particularly in the lower part of the active layer. © 2001 Elsevier Science B.V. All rights reserved.

Keywords: Kelvin–Helmholtz instability; Billows; Turbulent mixing; Night-time boundary layer

*Corresponding author. Tel.: +1-303-492-3770; fax: +1-303-492-3524.

E-mail address: blumen@paradox.colorado.edu (W. Blumen).

1. Introduction

The Cooperative Atmosphere–Surface Exchange Study (CASES-99) field observational program, carried out in the Great Plains of the United States during October 1999, was designed to obtain data that reveal the myriad of episodic events that characterize the night-time, stable boundary layer (NSBL). Further, it has been recognized that boundary layer parameterizations, which may be useful under fully convective conditions, are not suitable under conditions of both large static stability and large vertical wind shear, often observed in the NSBL. The type of events observed include: large- and small-amplitude internal gravity waves, inertial oscillations, density or gravity currents, shear flow instability and concomitant billows and intermittent turbulence near the ground and aloft, whose sources are not always evident, e.g. Nappo (1991). It is this intermittency associated with episodic events, as opposed to the more or less continuous turbulence and mixing that characterizes the fully convective regime, that has stymied progress on the development of viable parameterization schemes for the NSBL.

The various data need to be analyzed and models developed that will provide reliable depictions and predictions of the principal characteristics of the specific events observed during CASES-99. Direct numerical simulations (DNS) of stratified shear flow instability and turbulence are beginning to become commonplace, e.g. Werne and Fritts (1999). Yet, verification of model predictions has not been possible because the quantity and quality of atmospheric observations, which may be used for verification purposes, have not been available, e.g. De Silva et al. (1996). Laboratory experiments have filled a gap in data collection for this purpose, but this source does not necessarily replicate the most important aspects of turbulence and mixing that take place in the NSBL. The CASES-99 field observations are intended to be a first step in the acquisition of a data base that may be used to make quantitative comparisons between observations and models.

The present investigation focuses on an apparent initiation of a Kelvin–Helmholtz (KH) instability in a stably stratified shear flow in a relatively shallow surface-based layer. This KH instability is revealed by the structural evolution of a series of parallel roll vortices, referred to as KH billows, e.g. Fernando (1991). These billows are characterized by vorticity normal to the vertical mean shear flow. Their initial structure is wave-like; they steepen and begin to roll-up, concentrating their vorticity in roll vortices resembling a cat's-eye pattern, which typically extends through the depth of the shear layer. According to De Silva et al. (1996), “induced mixing (in the shear layer) requires an understanding of the initial evolution, breakdown and long-time evolution of KH billows”. The aim is to present quantitative observational data about the background flow and temperature structure that became unstable, the billow activity that emerged from this instability, and turbulence statistics that reveal some information about mixing processes within the layer containing the billow structures. More detailed heat and momentum flux calculations and comparisons with DNS model runs will be presented in future work.

The CASES-99 field site and instrumentation will be presented in Section 2. Section 3 provides observational evidence for the instability and billow activity observed just before midnight local standard time (6.00 UTC) on 6 October 1999. These data include temperature and wind profiles, lidar observations, and time series of temperature and winds from thermocouple and sonic anemometers mounted on a 60 m tower, which will be referred to as

the main tower. Characteristics of the atmospheric event, revealed by calculated Richardson numbers, billow height, length and speed, appear in Section 4. The turbulence statistics, which include variance and kurtosis in the active layer, are presented in Section 5. Final remarks appear in Section 6.

2. Site and instrumentation

The experimental design for CASES-99 is shown in Fig. 1. The main site in Leon, Kansas is embedded within two triangular regions, delineated by dashed lines. Boundary layer wind profilers, sodars and surface meteorological stations are maintained by the Argonne National Laboratory (ANL) at the vertices of the larger triangle. The smaller triangle, which shares the Beaumont facility, contains two additional boundary layer profilers installed by the National Center for Atmospheric Research (NCAR). Three NCAR radiosonde launch sites at each of the vertices of the smaller triangle provided wind, temperature and humidity data up to several kilometer above the ground.

The main site near Leon consists of a broad array of observational platforms, which include various remote sensors, a radiosonde, a tethered balloon and kite sounding systems, a 60 m tower, containing microbarographs, thermocouples, sonic, hot-film and hot-wire anemometers, and smaller towers with sonic instrumentation. Radiation, carbon dioxide and various soil measurements were also made. Poulos et al. (2001) have provided a more complete description of the goals of the program, the experimental design, a summary of the intensive observational periods (IOPs), and a summary of significant events observed.

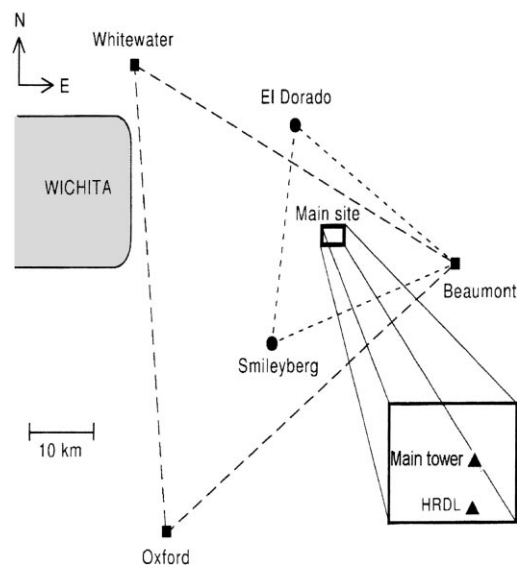


Fig. 1. Main CASES-99 site and outlying observational sites. Both radiosonde data and profiler wind data are available at El Dorado, Smileyberg, and Beaumont, but only profiler wind data are available at Whitewater and Oxford. The high resolution Doppler lidar (HRDL) site is approximately 1440 m south of the main tower.

Here, attention will be directed to the performance characteristics of the instrumentation used in the analysis of the instability/billow event observed on 6 October 1999. The instruments are thermocouples and sonic anemometers on the main tower, an NCAR radiosonde, and the high resolution Doppler lidar (HRDL), developed by the Environmental Technology Laboratory (ETL) of the National Oceanographic and Atmospheric Administration (NOAA). The tower is located near the center of the main site, and HRDL is located approximately 1440 m south of this facility. A radiosonde launch site was located close to the main tower, but radiosonde wind data were not available from this site near the time of the billow event. The closest sounding to the event, which obtained both wind and temperature data, was taken about 16 km to the north-northwest at El Dorado.

2.1. Radiosonde

The NCAR Global Positioning System (GPS) Loran Atmospheric Sounding System (GLASS) is the radiosonde facility used during CASES-99. Profiles of the atmospheric pressure, ambient temperature and relative humidity are obtained from expendable radiosondes suspended from a helium-filled balloon and sent back to a ground station via a radio transmitter. A meteorological surface station measures the same thermodynamic state variables at ground level. Wind speed and direction are measured by tracking the elevation and azimuth of the radiosonde using navigational aid signals from moving satellites in space. Data are obtained every second, or approximately every 5–10 m, depending on the rise rate of the balloon. Gaps in data acquisition exist at low-levels when the wind speed accelerates rapidly to a jet maximum at the top of the inversion; the GPS antenna on the sonde experiences difficulty in locking onto the three satellites required for a wind determination.

2.2. Doppler lidar

The high resolution Doppler lidar (HRDL) is a scanning coherent Doppler lidar that was specifically designed for atmospheric boundary layer (ABL) research. This instrument is similar in many respects to a Doppler weather radar. However, since the lidar operates in the near infrared, the scattering targets are aerosol particles, rather than hydrometeors or insects. Aerosols are widespread and well distributed in the lowest 2–4 km of the atmosphere and provide excellent tracers of the wind field. The Doppler lidar is, thus, useful for mapping the wind field in clear air.

HRDL measures range-resolved profiles of aerosol backscatter and radial velocity v_r , i.e. the component of velocity parallel to the beam. The pulse laser consists of a solid state (TmLu:YAG), injection seeded, Q-switched, laser transmitter operating at a wavelength of 2 μm and a 200 ns pulse width. The minimum range resolution is thus 30 m. During the CASES-99 deployment, the system was operated at a pulse repetition frequency of 200 Hz with a 2 mJ pulse energy. The lidar minimum range was 270 m for this project, and the maximum range, which is dependent on aerosol concentrations, was generally 2.0–2.5 km in the relatively clean night-time environment of central Kansas. The velocity precision is 10 cm s^{-1} for diffuse aerosol returns. Onboard computers provide the operator interface, data acquisition, scanner control and real-time Doppler signal processing capabilities. The entire lidar system is housed inside a sea-container, which is mounted on a trailer rig for

easy transport. Further design details of the HRDL system are given in Grund et al. (2001). Recent improvements to the frequency stabilization technique are described by Wulfmeyer et al. (2000).

The lidar beam can be scanned through the entire upper hemisphere, and a limited range of negative elevation angles. Beam steering is accomplished using a scanner mounted on the roof of the sea-container. The scanner has two degrees of rotational freedom, azimuth and elevation.

During the CASES-99 deployment, the strategy was to employ a variety of routine survey scans interspersed with higher angular resolution scans of features of interest. Routine survey scans generally consisted of plan-position-indicator (PPI) scans. These are scans performed by varying the azimuth angle of the lidar beam while maintaining a fixed elevation angle. Such scans are useful for surveying the horizontal structure of the velocity field and for computing vertical profiles of the mean horizontal wind components using the velocity-azimuth display (VAD) technique (Browning and Wexler, 1968). Alternatively, the range-height-indicator (RHI) or vertical-slice scan is useful for analyzing the structure of the velocity field in a two-dimensional vertical cross-section of the boundary layer. Vertical-slice scans are performed by varying the elevation angle of the lidar beam while maintaining a fixed azimuth angle. The lidar performed a series of vertical-slice scans in the general direction of the mean flow, in order to collect data during the period of the instability/billow event.

2.3. Thermocouple

E-type (chromel/constantan, 0.0254 mm diameter) thermocouples (Lee et al., 1997) were installed at 34 levels on the main tower and on two adjacent mini-towers. The thermocouple temperature was recorded at five samples per second with a vertical resolution of 1.8 m on the main tower from 2.3 to 58.1 m above the ground. The advantage of thermocouple temperature is its accuracy of the temperature difference between different vertical levels. The high accuracy of the thermocouple temperature is achieved by logging thermocouples from different vertical levels to the same data logger where a common reference temperature is used. The thin wires in the thermocouple probe ensures fast response time, which is very useful for measuring turbulent events. The thermocouple deployed in CASES-99 is the same as the one discussed in Cheney and Businger (1990), but with a different data logger. Assuming the performance of the Campbell CR23X data logger used in CASES-99 is similar to the data logger system used in Cheney and Businger (1990), the estimated accuracy for the thermocouple temperature difference is $\pm 0.01^\circ\text{C}$. According to the Campbell CR23X reference manual, the absolute accuracy of the reference thermistor is $\pm 0.25^\circ\text{C}$ for the range of $0\text{--}40^\circ\text{C}$. Comparisons of thermocouple, slow-response aspirated sensor, and sonic anemometer temperature data measured on the main tower indicate that the thermocouple data have the absolute accuracy of the aspirated sensor data and also capture the high-frequency temperature fluctuations revealed in the sonic data. Based on the aspirated-sensor and thermocouple temperature comparisons, the mean thermocouple temperature is about 0.1°C smaller than the aspirated temperatures during the night, and greater by 0.2°C during the day-time. These differences exist due to radiative-heating effects on the unshielded and un aspirated thermocouple sensors.

2.4. Sonic anemometer

The National Center for Atmospheric Research (NCAR) Atmospheric Technology Division (ATD) measured high-frequency vertical and horizontal wind components at the main tower with a combination of Campbell Scientific CSAT3 (at 1.5, 5, 30 and 50 m) and Applied Technologies “K” Style (at 10, 20, 40 and 55 m) sonic anemometers. These data were recorded at 20 samples per second.

3. Observations

HRDL and in situ tower sensors captured what appeared to be waves and turbulence associated with a shear instability over the CASES-99 field site between 5.20 and 5.45 UTC (23.20–23.45 local standard time) on 6 October 1999. The present aim is to use the available data to see where this CASES-99 wave event fits into our observational, theoretical, and numerical estimates of various characteristics of KH instability and billow development. The starting point will be an examination of the background wind and potential temperature profiles in order to establish that environmental conditions were suitable for this type of instability to occur. The tower and lidar data can provide the information at low-levels at the main CASES-99 site, but there were no radiosonde observations of the wind (only the temperature) available near the 5.20 UTC event time. A radiosonde observation taken at 3.00 UTC at a site located 16 km north-northwest of the main site is displayed in Fig. 2a. The flow was southerly, and the positive surface-based shear layer and inversion was confined to a depth of approximately 85 m. Winds at the surface were light ($<2 \text{ m s}^{-1}$). At this time, the Richardson number that characterizes the lowest 60 m layer in the El Dorado sounding was approximately 0.15. The potential temperature profile in Fig. 2b is based on radiosonde data obtained at the main site at 5.00 UTC, and the lidar wind-speed profile is based on data obtained between 5.30 and 5.50 UTC. The Richardson number profile, also shown in Fig. 2b, reveals that values below one-quarter extend through a depth of approximately 20 m at low-levels. The upper-level oscillation of the Richardson number is based on relatively small gradients of both potential temperature and wind speed, and may be spurious.

About 1 h prior to the billow event, the mean temperature gradient between the surface and the top of the main tower was approximately $0.14 \text{ }^\circ\text{Cm}^{-1}$, while the mean wind shear between 30 m and the top of the tower during the 15 min period prior to the event was approximately 0.17 s^{-1} . A series of large intermittent bursts in turbulence began at about 5.20 UTC and persisted until about 5.45 UTC, with the largest variance occurring above 20 m.

1 h time series of the temperature and horizontal and vertical wind speeds from tower data are presented in Fig. 3. The billow event is characterized by the larger amplitude 60 s period response during the interval 5.20–5.45 UTC. Although the atmosphere appears to be in a state that promotes instability a few hours before the 5.20 UTC event occurred, the observing systems in place did not record any other event that could be related to the onset of shear instability. This circumstance does not violate the theoretical underpinnings of the derived stability criterion, $Ri < 1/4$ (Howard, 1961). The condition $Ri < 1/4$ is a necessary, but not sufficient condition for the instability to occur, and weakly unstable events are expected to support only relatively slow unstable growth rates. Events similar to

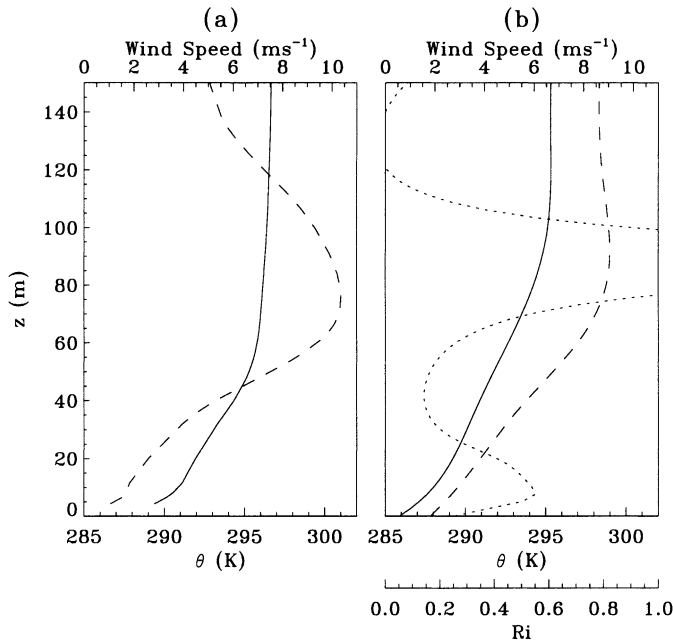


Fig. 2. Potential temperature (solid), wind speed (dashed) and Richardson number (dotted) based on: (a) the El Dorado radiosonde sounding at 3.00 UTC; (b) the main site radiosonde temperature sounding at 5.00 UTC and the lidar winds. The latter represent an average over all the vertical-slice (RHI) scans during the period 5.30–5.50 UTC. The potential temperature profiles represent a least-squares fit with a 16th-order Chebychev polynomial and the Richardson number profile, which appears in panel (b), is determined from local gradients calculated from the polynomial fit and the wind speed profile data.

the one observed may, however, have occurred outside the range of the CASES-99 observing systems.

Estimates of the Richardson number are based on mean profiles computed over 10 min periods of wind and potential temperature derived from tower sonic anemometers and thermocouples located between 25 and 55 m. The Richardson number is computed by determining an average gradient in wind speed and potential temperature over this height interval. The averaging periods were chosen to be 5.00–5.10 UTC prior to the event ($Ri \approx 0.13$), 5.25–5.35 UTC during the event ($Ri \approx 0.18$) and 5.50–6.00 UTC after the event, ($Ri \approx 0.15$).

Between 5.25 and 5.42 UTC, the lidar performed shallow vertical-slice scans in the general direction of the mean flow. The scan plane was oriented at an azimuth of 10° and the lidar scanned from 0 to 10° in elevation at a rate of $0.33^\circ \text{ s}^{-1}$, producing a full 10° scan in 30 s. As a result, the angular resolution of the scan was 0.083° . The lidar recorded 33 sequential scans during this period. Fig. 4 shows a representative sample of two vertical-slice scans taken with HRDL. The images display the structure of the radial velocity field in a vertical plane during two stages in the evolution of two different sets of billows. Positive radial velocities indicate flow away from the lidar. Coherent propagating wave structures are

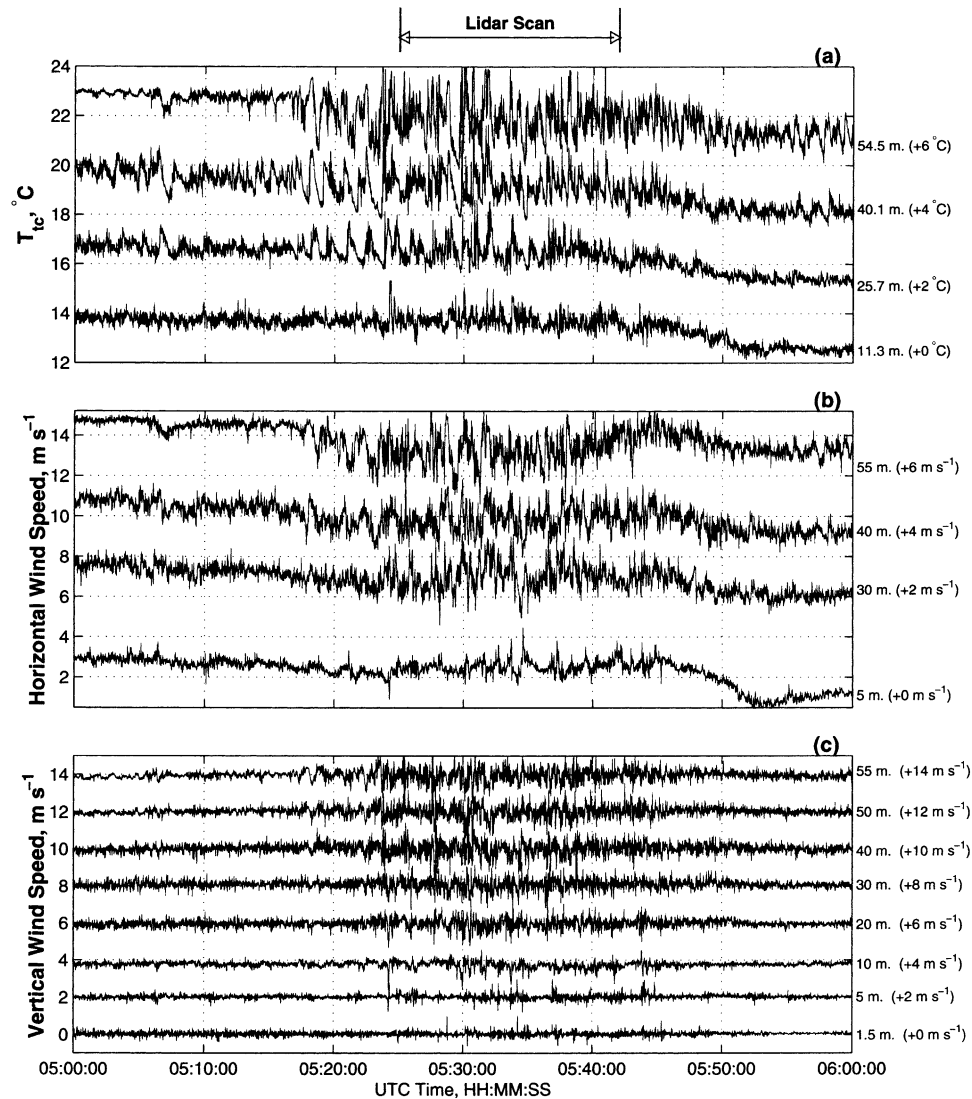


Fig. 3. Time series on 6 October 1999. (a) Thermocouple temperature; (b) sonic anemometer horizontal wind speed, and (c) sonic anemometer vertical wind speed. The instrument levels are indicated to the right of each series, and the numbers in parentheses indicate offsets required to avoid crossing of various lines.

clearly evident in animations of this scan sequence. In several scans, the lidar observations show distinct evidence of what appear to be overturning wave structures or billows.

The dominant wavelength of these features was determined by spectral analysis of the lidar scan data. When averaged over the entire sequence of scans this analysis indicates a peak in the spectral energy at a wavelength $L = 320$ m at $z = 56$ m. The phase speed was

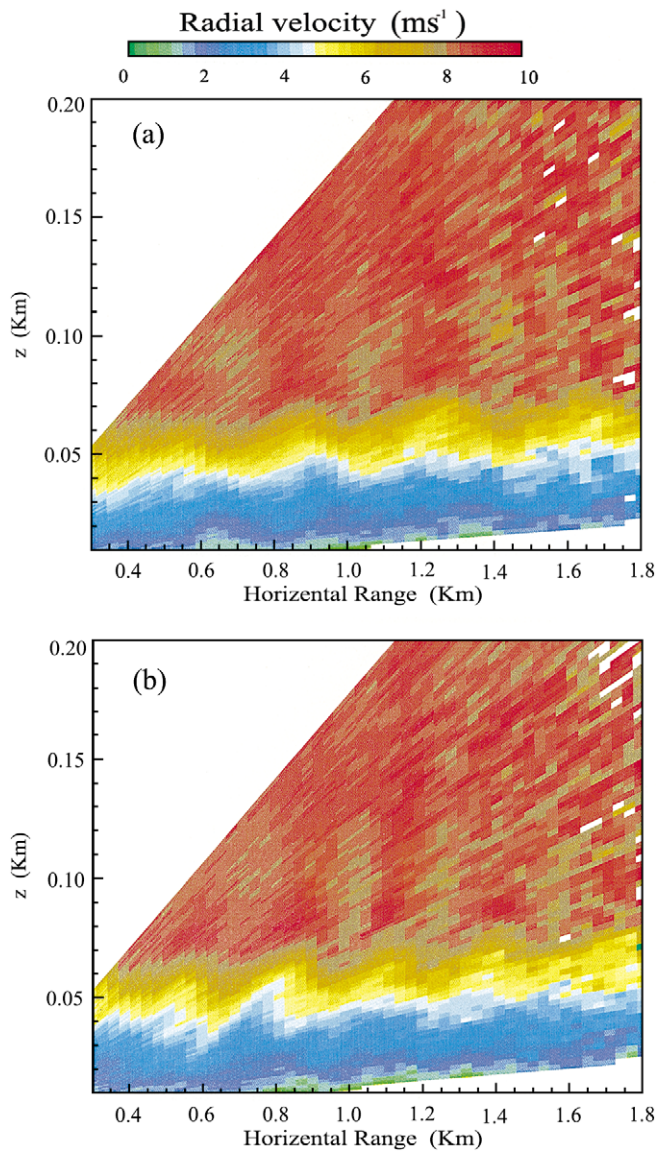


Fig. 4. Two representative vertical-slice (RHI) scans from HRDL illustrating the time-dependence of the structure of the waves. (a) Scan starting at 05:30:49 UTC: note central wave at $x = 0.9$ km is just starting to break; (b) scan starting at 05:34:24 UTC: note that wave at $x = 0.75$ km is in an advanced stage of overturning. The vertical axis is stretched, so that the x -axis extends to 1.8 km from the lidar, whereas the z -axis extends to 200 m AGL.

estimated using two techniques. First, individual wave crests were visually tracked through several successive scans. This yielded a phase speed of 5.5 m s^{-1} . Second, a slightly more sophisticated approach involved fitting a traveling wave of the form $\exp(ik(x - ct))$ to the lidar data at the height of maximum wave amplitude using least-squares minimization. This method accounts for the non-simultaneity of individual radial velocity estimates within a given scan. The phase speed obtained from this technique was 5.4 m s^{-1} for the dominant wavelength ($L = 320 \text{ m}$). The vertical profile of the mean velocity component projected into the lidar scan plane was estimated by dividing the radial velocity by the cosine of the elevation angle. This approximation is valid provided the elevation angle is small or the vertical velocity is much smaller than the horizontal component parallel to the scan plane. In this case, the maximum elevation angle of the lidar scan was 10° . The scan plane was oriented at an azimuth of 10° and the mean wind direction was southerly above 40 m . It should be pointed out that near the surface, the wind direction was south-southeasterly. Nevertheless, the horizontal scan plane wind component provides a reasonable approximation to the streamwise component and provides useful information regarding the vertical dependence of the horizontal wave amplitude. Fig. 5 shows vertical profiles of the mean (solid line) and variance (dashed line) of the approximate streamwise velocity derived from the lidar scan

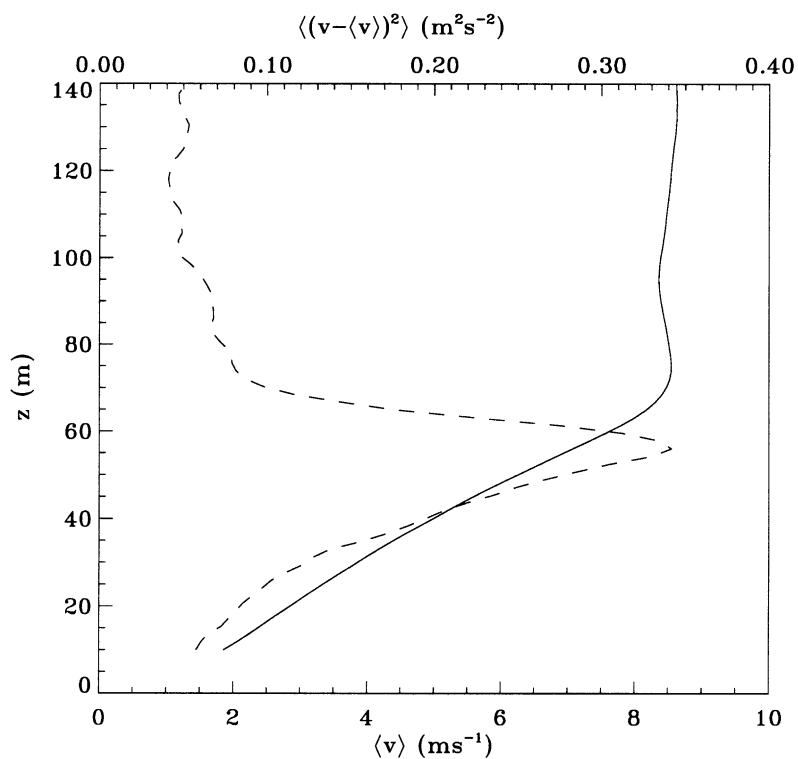


Fig. 5. Vertical profiles to the mean (solid) and variance (dashed) of the streamwise velocity component, calculated from repeated vertical-slice HRDL scan data taken between 5.25 and 5.43 UTC.

data. Radial velocity estimates were processed using 60 m range gates. As a result of the spatial averaging inherent in the lidar data, the dominant contribution to the variance comes from the wave-scale motion in the horizontal direction. In this case, the variance profile indicates a maximum wave amplitude at $z = 56$ m. Most of the wave energy, as determined by the half-width of the variance curve is concentrated between roughly 35 and 65 m AGL. The mean streamwise velocity profile increases monotonically up to ~ 70 m AGL. An inflection point in this profile occurs at the same location of the peak variance, $z = 56$ m, providing a necessary condition for instability (Synge, 1933). Also, the mean streamwise component is approximately 7 m s^{-1} at this level. This observation is in agreement with predictions of the semi-circle theorem (Howard, 1961) that the real part of the phase speed lies within the unstable portion of the flow.

The waves are expected to propagate in the direction of the wind shear vector at the height of minimum Richardson number (De Bass and Driedonks, 1985). The height of the inflection point in the velocity profile shown in Fig. 5 occurs in a region where the potential temperature gradient is approximately constant. This implies a minimum in the Richardson number at this height, since the wind shear has a maximum there. The direction of the wind-shear vector at this height was found to be approximately 15° , i.e. the waves should propagate from an azimuth of 195° .

4. Characteristics of the event

Fernando (1991) and Scorer (1997) note that Kelvin–Helmholtz, or stratified shear flow instability is a necessary precursor to billow formation. As stated by Scorer, “The vorticity is collected into nodes by the instability and the layer is rolled up into billows, which is the name given to this phenomenon to distinguish it from gravity waves caused by an outside disturbance such as a hump in the boundary or violent convection. Billows always occur several at a time, and are the principal cause of mixing in a stably stratified medium”. Observations from remote sensors and numerical modeling results appear to support Scorer’s view at least at lower levels of the atmosphere. It is desirable to use the CASES-99 observations to compare the thickness of the billow layer or the billow amplitude h , and the billow wavelength L , to theoretical and model-derived values of h/L . This will provide insights to the stage of development of the billows, dependence on the Richardson number, etc. The present data exhibit some limitations. For example, the lidar measurements show that the billow activity extended above the height of the main tower, but reliable in situ wind and temperature observations are available only from the tower instrumentation at the time of the event. In addition, some estimates of h/L are made using vortex sheet models to generate the instability, which is a simplification of real atmospheric structure. In the present case there is a Richardson number dependence to be considered. Some models do not take into account the presence of the lower boundary, which may alter the instability characteristics, and consequently the billow structure which develops. Early observational studies with radar (Atlas et al., 1970), cloud photography (Ludlum, 1967) and observations from an instrumented tower (Hooke et al., 1973), all seem to indicate some agreement regarding the features of lower tropospheric billows. The wavelength L is usually less than 1 km, but could be longer. The value of h/L is less than unity, and the period of billow activity

Table 1

Value of H/L , for fixed L , associated with indicated ranges of Ri , e.g. Thorpe (1973) and De Silva et al. (1996)

$Ri \lesssim 0.05$	$H/L \gtrsim 0.50$
$0.10 \lesssim Ri \lesssim 0.15$	$0.15 \lesssim H/L \lesssim 0.40$
$Ri \gtrsim 0.15$	$0.10 \lesssim H/L$

is often confined to 15–30 min. We now examine how our present observations compare with laboratory, theoretical, and numerical models of KH instability.

Early theoretical studies showed that the wavelength and character of the motion having the maximum linear growth rate depend on the mean velocity and stability profiles and the presence of a rigid lower boundary (Drazin, 1958; Miles and Howard, 1964; Lalas and Eiuaudi, 1976; Davis and Peltier, 1976). Typical values of wavelength range from $L \sim 2\pi h$ to $7.5h$, where h is the depth of the shear layer (Miles and Howard, 1964; Scorer, 1997; Werne and Fritts, 1999). The depth to which the shear layer mixes also depends on the characteristics and initial instability of the flow. Laboratory and initial two-dimensional (2D) numerical studies revealed a dependence of maximum billow amplitude on both Richardson number and Reynolds number, with larger billows and deeper implied mixing layers accompanying smaller Ri and larger Re (Thorpe, 1973; Patnaik et al., 1976; Peltier et al., 1979; Klaassen and Peltier, 1985). These results were confirmed and extended in recent three-dimensional (3D) modeling studies of KH instability and transition to turbulence (Palmer et al., 1994, 1996; Caulfield and Peltier, 1994; Fritts et al., 1996; Werne and Fritts, 1999; Smyth, 1999). In particular, these studies noted a tendency for billow and mixed layer depth, H , to vary inversely with Ri for fixed L , as displayed in Table 1.

Application to our CASES-99 measurements, indicate a shear depth following billow evolution of ~ 70 m, or $H/L \sim 0.18$, in reasonable agreement with the results of Thorpe (1973) for an initial $Ri \sim 0.15$. In other respects, we also observe good agreement with our theoretical and numerical understanding of KH instability. Both the wave number vector and the maximum horizontal velocity variance were nearly aligned with the direction of maximum shear, while the maximum variance with altitude occurred very close to the height of maximum shear at ~ 60 m.

5. Turbulence statistics

Tower measurements clearly indicate a substantial increase in turbulence activity between 5.15 and 5.45 UTC on 6 October. Variance spectra computed from thermocouple temperature data between 20 and 60 m during the most active period (5.18–5.42 UTC) indicate that the dominant wave period was approximately 60 s. Fig. 6 shows time–height displays of vertical velocity w variance and the kurtosis of both the vertical and horizontal wind speeds. These data were obtained by first high-pass filtering the sonic data to reduce trends in the signal over the averaging period. The averaging period was chosen to be 20 s to adequately resolve changes in small-scale turbulent fluctuations with the passage of individual billows. The vertical velocity variances displayed in the upper panel of Fig. 6 reveal approximately periodic enhancements at 60–80 s intervals and larger values near the top of the tower. These

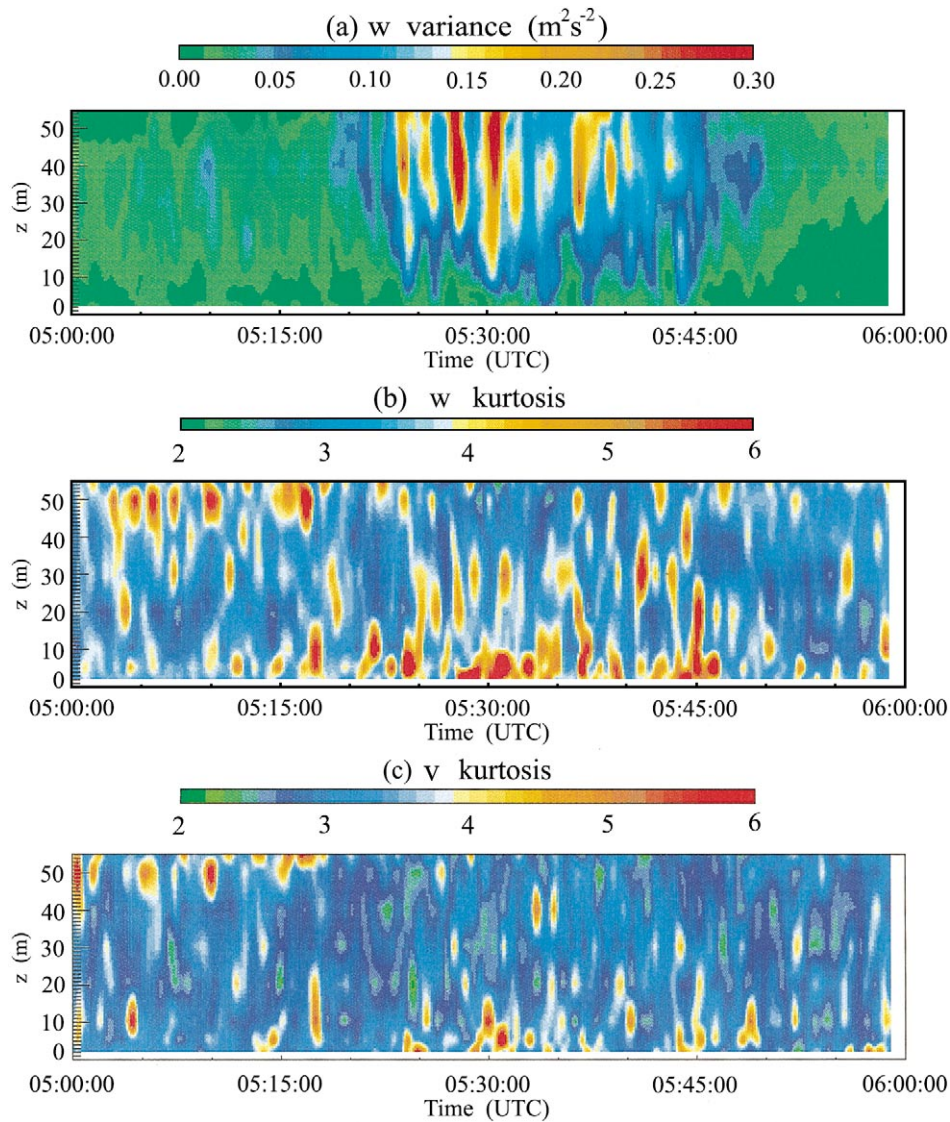


Fig. 6. Height–time displays of turbulence statistics derived from sonic data on the main tower: (a) variance; (b) w kurtosis; (c) v kurtosis. Variances and kurtosis were computed using 20 s averaging times. Measurements have been linearly interpolated between anemometer levels, which were located at $z = 1.5, 5, 10, 20, 30, 40, 50$ and 55 m.

data are consistent with the turbulence expected to accompany KH billow activity during the breakdown phase.

Kurtosis of the vertical and horizontal velocity components was computed in 20 s intervals in order to relate its variations to the variations in billow turbulence and vertical

velocity variance. Kurtosis provides an indication of the degree of intermittency of turbulence and mixing and has a value of 3 for a Gaussian distribution, with larger values indicative of greater intermittency and more extreme velocities. In the simulations described by Werne and Fritts (1999), large values of kurtosis were found to be associated with high intermittency of velocities and velocity gradients in regions of active entrainment dynamics at the edges of the turbulent layer. In the middle and lower panels of Fig. 6, velocity kurtosis during the billow event is seen to exhibit maxima preferentially at the lowest altitudes and at the edges of the billows having the largest velocity variances. Peak values approach 15 and 8, respectively, for the w and v kurtosis in association with the billow turbulence extending from 5.28 to 5.32 UTC. By analogy with the numerical simulations of Werne and Fritts (1999), these regions would appear to be the sites of most vigorous entrainment and mixing dynamics at the edges of fully turbulent billows. The elevated values of kurtosis at the lowest altitudes at later times (extending to 5.47 UTC) are likewise consistent with the numerical simulations and may indicate continuing entrainment and mixing following billow collapse and horizontal homogenization of the shear layer.

6. Final remarks

The CASES-99 instrumentation and deployment was designed to obtain data from high-frequency measurement systems positioned on a 60 m tower and on surrounding 10 m towers, and from a variety of remote sensors. High-frequency thermocouple and sonic anemometer data from the main tower and the high resolution Doppler lidar (HRDL) observations were used for the present analysis. Other data (e.g. hot-film and hot-wire anemometers) will be examined when all the data sources become available. Regretably aircraft traverses cannot be used for low-level events below 150 m in night-time operations, although these data would not be useful in the present case.

It has been established that the atmospheric environment was conducive to stratified shear instability during the 2–3 h period prior to the onset of the observed billow activity. It is quite possible that this type of activity occurred elsewhere at earlier times, but this speculation cannot be confirmed. Yet, the characteristics of the billow activity observed are consistent with the length of time that billows, associated with KH instability, have been observed in the Earth's atmosphere, their characteristic wavelength, and the depth of the layer in which they are embedded. In addition, theoretical constraints providing necessary conditions for the instability are satisfied by the present observations.

Both horizontal and vertical velocity variances provided strong indications of billow structure and turbulence, while velocity kurtosis maximized (1) at the edges of billows exhibiting strong turbulence and (2) at the lower edge of the turbulent layer following billow collapse. Together, these data suggest strong parallels with the numerical simulations of KH instability and turbulence by Werne and Fritts (1999) and important mixing and entrainment dynamics within the nocturnal boundary layer due to KH instability. A more quantitative evaluation, however, will require computation of the temporal evolution of heat and momentum fluxes and numerical studies specifically targeting this and other such events.

Acknowledgements

Financial support is provided, in part, to WB by the Atmospheric Sciences Division, Mesoscale Dynamics Program of the National Science Foundation (NSF), WB, DF and GSP gratefully acknowledge support from the Army Research Office, Mechanical and Environmental Sciences Division, contract DAAD 19-99-C-0037. GSP also acknowledges support from the Department of Energy, Environmental Meteorology Program, contract DE-FGO3-99ER62839, and DF also acknowledges support from the NSF, grant ATM 9908615. JS and SB are supported by the US Army Research Office (ARO), contract DAAD19-99-1-0320, and NSF, grant ATM-9906637. HRDL was developed by the NOAA ETL, in conjunction with NCAR, with funding provided by ARO. Deployment of HRDL and analysis funding for RB and RN were provided by ARO under proposal no. 40065-EV, by the Cooperative Institute for Research in the Atmosphere (CIRA), and by the National Science Foundation under grant no. ATM9908453. We thank the following individuals for their role in data acquisition during CASES-99: Scott Sandberg, Wynn Eberhard, Jeff Otten, Joanne George, Max Pichugin, Volker Wulfmeyer, Allen Brewer, Ann Weickmann, and Julie Lundquist. We wish to express our appreciation to the many individuals, too numerous to list individually, who helped to set up all the facilities for the CASES-99 field program, but especially Jerry Klazura, Gordon Maclean and Steve Oncley. We also thank X. Lee and Xinzhang Hu, Yale University, for assembling the thermocouples. The National Center for Atmospheric Research is sponsored by the National Science Foundation.

References

- Atlas, D., Metcalf, J.I., Richter, J.H., Gossard, E.E., 1970. The birth of “CAT” and microscale turbulence. *J. Atmos. Sci.* 27, 903–913.
- Browning, K.A., Wexler, R., 1968. The determination of kinematic properties of a wind field using Doppler radar. *J. Appl. Meteor.* 7, 105–113.
- Caulfield, C.P., Peltier, W.R., 1994. Three-dimensionalization of the stratified mixing layer. *Phys. Fluids* 6, 3803–3805.
- Cheney, N.R., Businger, J.A., 1990. An accurate fast response temperature system using thermocouples. *J. Atmos. Ocean. Technol.* 7, 504–516.
- Davis, P.A., Peltier, W.R., 1976. Resonant parallel shear instability in the stably stratified planetary boundary layer. *J. Atmos. Sci.* 33, 1287–1300.
- De Bass, A.F., Driedonks, G.M., 1985. Internal gravity waves in a stably stratified boundary layer. *Bound.-Layer Meteorol.* 31, 303–323.
- De Silva, L.P.D., Fernando, H.J.S., Eaton, F., Hebert, D., 1996. Evolution of Kelvin–Helmholtz billows in nature and laboratory. *Earth Plan. Sci. Lett.* 143, 217–231.
- Drazin, P.G., 1958. The stability of a shear layer in an unbounded heterogeneous inviscid fluid. *J. Fluid Mech.* 4, 214–224.
- Fernando, H.J.S., 1991. Turbulent mixing in stratified fluids. *Ann. Rev. Fluid Mech.* 23, 455–493.
- Fritts, D.C., Palmer, T.L., Andreassen, O., Lie, I., 1996. Evolution and breakdown of Kelvin–Helmholtz billows in stratified compressible flows. Part 1: comparison of two- and three-dimensional flows. *J. Atmos. Sci.* 22, 3173–3191.
- Grund, C.J., Banta, R.M., George, J.L., Howell, J.N., Post, M.J., Richter, R.A., Weickmann, A.M., 2001. High-resolution Doppler lidar for boundary-layer and cloud research. *J. Atmos. Oceanic Technol.* 18, 376–393.
- Hooke, W.H., Hall, F.F., Gossard, E.E., 1973. Observed generation of one atmospheric gravity wave by shear instability in the mean flow of the planetary boundary layer. *Bound.-Layer Meteorol.* 5, 29–41.

- Howard, L.N., 1961. Note on a paper by John Miles. *J. Fluid Mech.* 10, 509–512.
- Klaassen, G.P., Peltier, W.R., 1985. The onset of turbulence in finite-amplitude Kelvin–Helmholtz billows. *J. Fluid Mech.* 155, 1–35.
- Lalas, D.P., Eiuaudi, F., 1976. On characteristics of gravity waves generated by atmospheric shear layers. *J. Atmos. Sci.* 33, 1248–1259.
- Lee, X., Neumann, R.H., Den Hartog, G., Fuentes, J.D., Black, T.A., Mickle, R.E., Yang, P.C., Blanken, P.D., 1997. Observation of gravity waves in a boreal forest. *Bound.-Layer Meteorol.* 84, 383–398.
- Ludlum, F.H., 1967. Characteristics of billow clouds and their relation to clear air turbulence. *Q. J. R. Meteor.* 93, 419–436.
- Miles, J.W., Howard, L.N., 1964. Note on heterogeneous shear flow. *J. Fluid Mech.* 20, 331–336.
- Nappo, C.J., 1991. Sporadic breakdowns of stability in the PBL over simple and complex terrain. *Bound.-Layer Meteor.* 54, 69–87.
- Palmer, T.L., Fritts, D.C., Andreassen, O., Lie, I., 1994. Three-dimensional evolution of Kelvin–Helmholtz billows in stratified compressible flow. *Geophys. Res. Lett.* 21, 2287–2290.
- Palmer, T.L., Fritts, D.C., Andreassen, O., 1996. Evolution and breakdown of Kelvin–Helmholtz billows in stratified compressible flows. Part II: Instability structure, evolution and energetics. *J. Atmos. Sci.* 53, 3192–3212.
- Patnaik, P.C., Sherman, F.S., Corocos, G.M., 1976. A numerical simulation of Kelvin–Helmholtz waves of finite amplitude. *J. Fluid Mech.* 73, 215–240.
- Peltier, W.R., Halle, J.R., Clark, T.L., 1979. The evolution of finite amplitude Kelvin–Helmholtz billows. *Geophys. Astrophys. Fluid Dyn.* 10, 53–87.
- Poulos, G.S., Blumen, W., Fritts, D.C., Lundquist, J.K., Sun, J., Burns, S., Nappo, C., Banta, R., Newsom, R., Cuxart, J., Terradellas, E., Balsley, B., Jensen, M., 2001. CASES-99: A comprehensive investigation of the stable nocturnal boundary layer, *Bull. Am. Meteor. Soc.*, submitted for publication.
- Scorer, R.S., 1997. *Dynamics of meteorology and climate*. Wiley, Chichester, UK, 686 pp.
- Smyth, W.D., 1999. Dissipation-range geometry and scalar spectra in sheared stratified turbulence. *J. Fluid Mech.* 401, 209–242.
- Synge, J.L., 1933. The stability of heterogeneous liquids. *Trans. R. Soc. Canada* 27, 1–18.
- Thorpe, S.A., 1973. Experiments on instability and turbulence in stratified shear flow. *J. Fluid Mech.* 61, 731–751.
- Werne, J., Fritts, D.C., 1999. Stratified shear turbulence: evolution and statistics. *Geophys. Res. Lett.* 26, 439–442.
- Wulfmeyer, V., Randall, M., Brewer, W.A., Hardesty, R.M., 2000. 2 μm Doppler lidar transmitter with high frequency stability and low chirp. *Opt. Lett.* 25, 1228–1230.